Revealing highly complex elastic nonlinear (anelastic) behavior of Earth materials applying a new probe: Dynamic acoustoelastic testing

G. Renaud,[1] P.-Y. Le Bas,[2] and P. A. Johnson[2]

Received 26 December 2011; revised 18 April 2012; accepted 20 April 2012; published 6 June 2012.

[1] Recent work in medical nonlinear acoustics has led to the development of refined experimental method to measure material elastic nonlinear (anelastic) response. The technique, termed dynamic acoustoelastic testing, has significant implications for the development of a physics-based theory because it provides information that existing methods cannot. It provides the means to dynamically study the velocity-strain and attenuation-strain relations through the full wave cycle in contrast to most methods that measure average response. The method relies on vibrating a sample at low frequency in order to cycle it through different levels of stress-strain. Simultaneously, an ultrasonic source applies pulses and the change in wave speed and attenuation as a function of the low frequency strain is measured. We report preliminary results in eleven room-dry rock samples. In crystalline rock, we expect that the elastic nonlinearity arises from the microcracks and dislocations contained within individual crystals. In contrast, sedimentary rocks may have other origins of elastic nonlinearity, currently under debate. A large quadratic elastic nonlinearity is observed in Berkeley blue granite, presumably due to microcracks and dislocation-point defect interactions. In sedimentary rocks that include limestones and sandstones we observe behaviors that can differ markedly from the granite, potentially indicating different mechanical mechanisms. We further observe changes in measured nonlinear coefficients that are wave-strain amplitude dependent. Ultimately we hope that the new approach will provide the means to quantitatively relate material nonlinear elastic behavior to the responsible features, that include soft bonds dislocations, microcracks, and the modulating influences of water content, temperature and pressure.

Citation: Renaud, G., P.-Y. Le Bas, and P. A. Johnson (2012), Revealing highly complex elastic nonlinear (anelastic) behavior of Earth materials applying a new probe: Dynamic acoustoelastic testing, *J. Geophys. Res.*, *117*, B06202, doi:10.1029/2011JB009127.

1. Introduction

[2] Unraveling the physics of the earthquake source, reliable sequestration of CO_2, predicting wellbore breakout in oil and gas reservoirs, monitoring thermal damage to rock in nuclear waste storage, and probing cement integrity require new approaches to material characterization and imaging. The elastic nonlinear material response (also known as the anelastic response) is extremely promising in this regard [*Guyer and Johnson*, 2009]; however, a persistent problem has been the direct relation between elastic nonlinearity and material integrity, the primary contribution to elastic nonlinearity [e.g., *Guyer and Johnson*, 2009], because a reliable physics-based theory linking the two does not yet exist. Recent work in medical nonlinear acoustics has led to the development of a hybrid experimental method to measure material nonlinear response. The technique, termed dynamic acoustoelastic testing (DAET) [*Renaud et al.*, 2008, 2009; *Moreschi et al.*, 2010], has significant implication for the development of a physics-based theory, and thus ultimately to our ability to directly relate nonlinear material behavior to features that may be responsible for the elastic nonlinear response, that include soft bonds, dislocations, microcracks, etc. The method relies on exciting a sample with a low frequency vibration in order to cycle it through stress-strain multiple times. Simultaneously, a high frequency ultrasonic source applies pulses that probe changes in wave speed and in attenuation as a function of the low frequency strain. The approach is directly analogous to measuring wave speed as a function of applied static load [*Winkler and McGowan*, 2004], but can be used at modest vibrational strains, can be very applied quickly and can measure changes through tensile and compressive strain.

[1]Department of Biomechanical Engineering, Erasmus Medical Center, Rotterdam, Netherlands.
[2]Earth and Environmental Sciences, Los Alamos National Laboratory, Los Alamos, New Mexico, USA.

Corresponding author: G. Renaud, Department of Biomechanical Engineering, ThoraxCenter, Erasmus Medical Center, Rotterdam 3000 CA, Netherlands. (renaud_gu@yahoo.fr)

0148-0227/12/2011JB009127

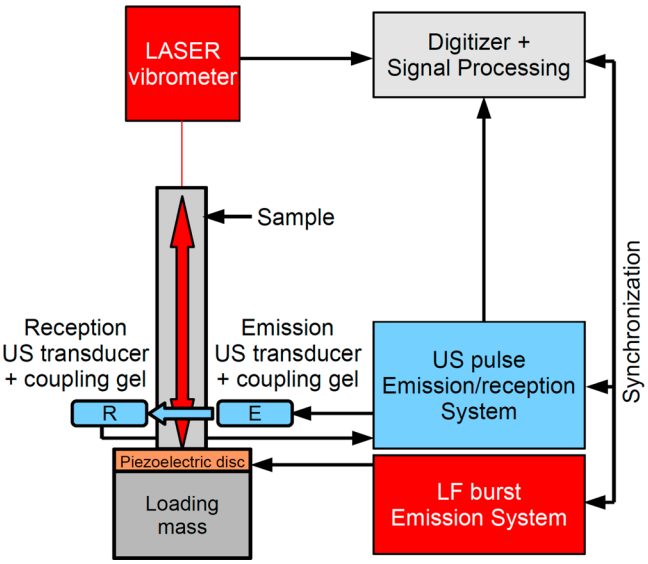

Figure 1. Experimental setup to perform dynamic acoustoelastic testing.

Thus it may prove particularly useful for investigating properties related to situations when one or more of the principal stresses is tensile (hydrofracturing, explosive loading/unloading, deformed rocks at a free surface). Applying signal averaging over multiple vibrational cycles leads to significant signal-to-noise ratio and robust statistics regarding the calculation of the complex modulus. Earlier studies applied similar techniques to characterize fatigue damage in polymers and metals [*Nagy*, 1998], or dislocations in metals [*Gremaud et al.*, 1987]. Nagy applied flexural resonance. Gremaud's method is essentially identical to DAET, except that the sample is loaded by a compressive stress applied in a quasi-static manner.

[3] In crystalline rock, we expect that the elastic nonlinearity arises due to microcracks as well as dislocations contained within individual crystals. In contrast, sandstones, limestones and other sedimentary rocks may have other origin(s) of elastic nonlinearity that are under debate. Thus as a first step, we can use a crystalline sample as a reference from which to extrapolate to other sources of nonlinear mechanisms. More sophisticated measures of standards with known origins of elastic nonlinearity are in progress. We report results from our preliminary studies in room-dry rock samples of differing rock types including Berkeley blue granite (Elberton, Georgia). We compare results to those obtained from sandstones, limestones and a soapstone. In section 2, we describe the approach. In section 3, we show the measurements of the ultrasound wave speed and attenuation as functions of the low frequency strain and strain rate, and amplitude dependence on vibration. We then interpret what the differences in the elastic nonlinearity mean. New insights obtained from the technique are discussed in section 4.

2. Dynamic Acoustoelastic Testing

[4] In dynamic acoustoelastic testing (DAET), a sample is simultaneously probed by two elastic waves that interact due to material elastic nonlinearity [*Renaud et al.*, 2009, 2011] (Figure 1). A sequence of ultrasound (US) pulses are applied simultaneously with a low-frequency (LF) standing wave generated by a piezoelectric source attached to one end of the cylindrical sample. DAET requires the LF wave to be quasi-static over the US Time Of Flight (TOF) interval and quasi-uniform in the probed volume that is the intersection volume between the LF and US strain fields. As a result, the LF period must be at least ten times higher than the US TOF [*Renaud et al.*, 2008] and the low frequency is selected to match with the frequency of the lowest-order longitudinal resonance mode of the cylinder. A heavy steel backload attached to the piezoelectric disc driving the LF excitation imposes fixed-free boundary conditions (Figure 1). Thus the resonance mode is such that the length of the sample L equals a quarter of the LF wavelength λ_{LF}, $L = \lambda_{LF}/4$. Consequently the LF strain field is quasi-uniform along the US propagation path. The LF axial strain undergone by the region of the sample probed by the US pulses is deduced from the acoustic particle velocity measured at the free end of the sample by a laser vibrometer (Figure 1). Two disc-shaped 6 mm-diameter US transducers are used to generate and receive pulses in the frequency range from1 MHz to 2 MHz. Coupling gel (water-soluble ultrasound transmission gel) is applied between the sample and transducers such that they are not in direct mechanical contact. A thin layer of nail polish is placed on the investigated area so that the gel does not penetrate into the rock via capillarity action.

[5] The repetition rate of the US pulses is selected based on the ultrasonic properties of the samples and so that there is no overlap of the coda of each pulse with the following pulse. Here the repetition rate ranges between 1 kHz and 6 kHz. The ratio between the pulse repetition rate and the frequency of the LF resonance must not equal a rational number so that US pulses probe different LF strains (equivalent to vibrational phase) during each LF cycle. In this manner, over roughly one hundred LF periods, US pulses probe discrete values well distributed over the entire LF strain excursion, both in tension and in compression. In between each measurement, the sample rests for at least 30 s to ensure relaxation (the slow dynamics [e.g., *Ten Cate and Shankland*, 1996; *Ten Cate et al.*, 2000]) of the rock after it has been conditioned by the LF excitation (the slow dynamics continues considerably longer than 30 s, but most of the relaxation takes place within the first 30 s). The triggering of the 80 ms LF excitation is delayed by 50 ms such that the first US pulses propagate through the sample without the influence of the LF standing wave. This unperturbed signal is used as a reference for the US TOF and amplitude. For each US pulse, the Time Of Flight Modulation (TOFM) and the Relative Amplitude Modulation (RAM) are computed [*Renaud et al.*, 2008, 2009, 2011]. TOFM is determined by the time position of the maximum of the cross-correlation function between the current US pulse and the very first US reference pulse (Figures 2a and 2b). The peak of the cross-correlation function is interpolated by a second-order polynomial function to achieve sub-sample time delay estimation [*Céspedes et al.*, 1995]. Thus a TOFM of less than 1 ns can be detected whereas the sampling period of the signal is 20 ns. In addition, the Fourier transform of each US pulse is computed to calculate its amplitude A as the peak value of the frequency spectrum

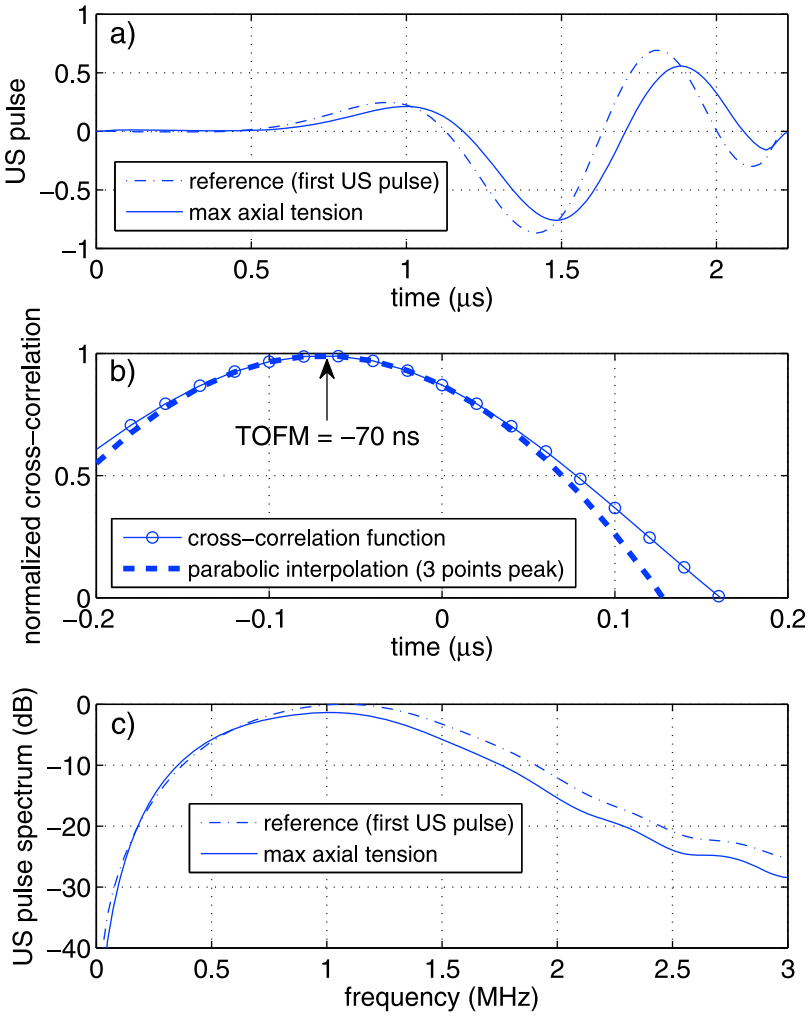

Figure 2. Measurement of time of flight modulation (TOFM) and amplitude modulation of US pulses in Berea sandstone. (a) Reference time signal (the reference is taken when the rock is at equilibrium conditions) and delayed time signal undergoing an axial tensile strain of 8×10^{-6}. (b) Peak of the normalized cross-correlation function between the US pulse undergoing the axial tensile strain of 8×10^{-6} and the reference US pulse shown in Figure 2a. (c) Frequency spectra of the reference and perturbed US pulses shown in Figure 2a used to calculate the variation in US pulse amplitude. The parabolic interpolation applied to the peak of the cross-correlation function to provide sub-sample estimation of TOFM is depicted in Figure 2b.

(Figure 2c). Thus for each US pulse with index i, $TOFM(i)$ and $RAM(i)$ are defined as

$$TOFM(i) = TOF(i) - TOF(1), \tag{1}$$

$$RAM(i) = [A(i) - A(1)]/A(1). \tag{2}$$

[6] The computation of TOFM and RAM is performed in a fixed time window including the received signal corresponding to the direct transmission (first two periods of the received US signal). Each US pulse is then associated with the value of the axial LF strain experienced by the material during its TOF in the sample ϵ_{LF}. Because of the high elastic nonlinearity exhibited by rock samples, the effects of the small dynamically induced changes in the sample dimensions and in the density can be neglected [*Renaud et al.*, 2011]. Thus TOFM can be related to variations in the elastic modulus M governing the US propagation in the sample as follows [*Renaud et al.*, 2011]:

$$\frac{M(\epsilon_{LF}) - M_0}{M_0} = \frac{\Delta M(\epsilon_{LF})}{M_0} \approx -\frac{2}{TOF_0} TOFM. \tag{3}$$

RAM can be related to variations in the US attenuation α as follows:

$$RAM = \frac{e^{(-\alpha(\epsilon_{LF})d)} - e^{(-\alpha_0 d)}}{e^{(-\alpha_0 d)}}, \tag{4}$$

$$\alpha(\epsilon_{LF}) - \alpha_0 = \Delta\alpha(\epsilon_{LF}) = -\ln(1 + RAM)/d, \tag{5}$$

where d is the US propagation distance in the sample. The subscript 0 indicates the value of US parameters in the

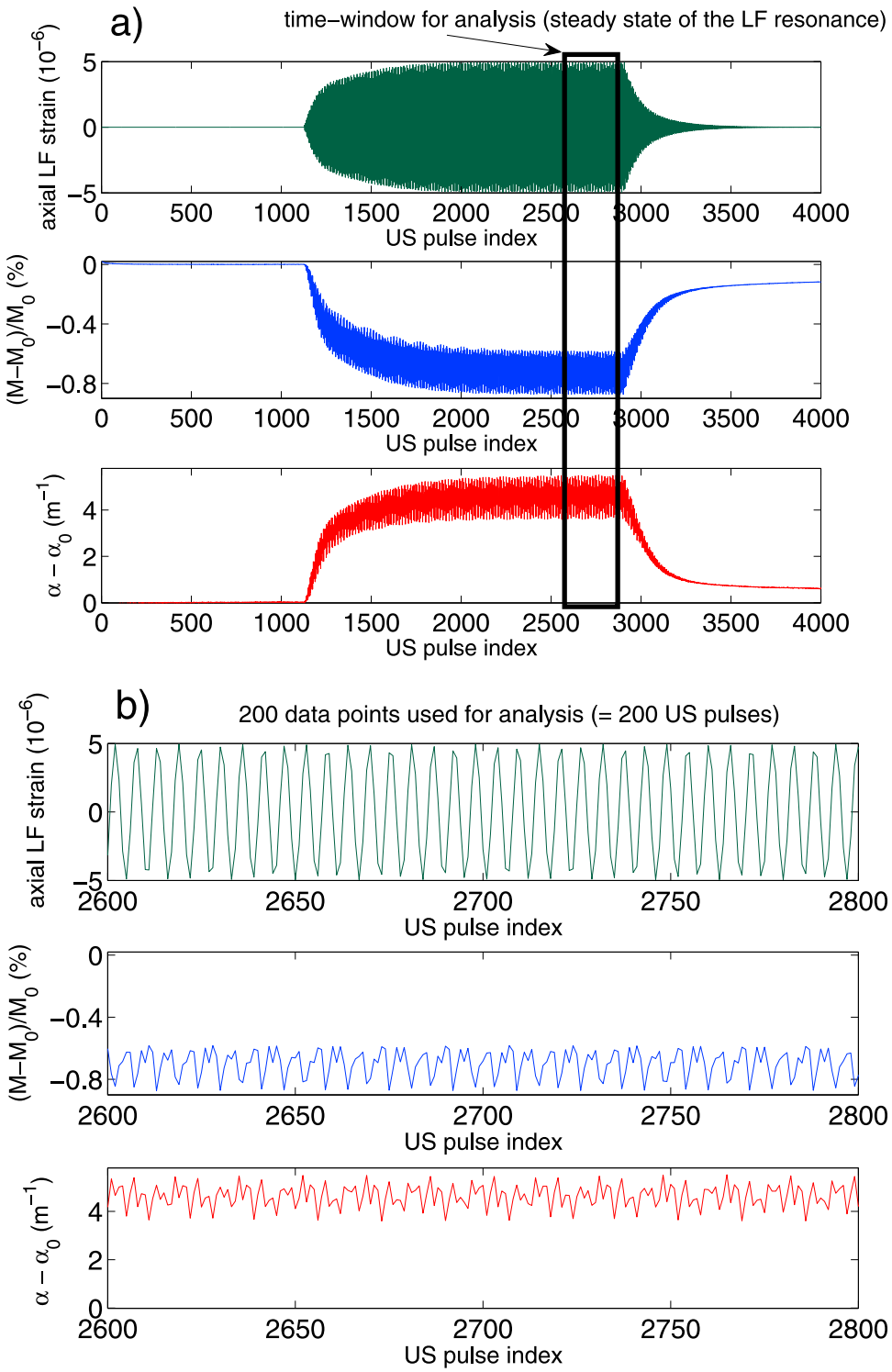

Figure 3. (a) Axial LF strain, variation in the elastic modulus and variation in the US attenuation as functions of US pulse index (or time) measured in Berea sandstone for an axial LF strain amplitude of 5×10^{-6}. (b) Expanded view during the steady state of the LF resonance showing the 200 data points used for the analysis. The pulse repetition rate is 25 kHz.

absence of LF resonance. As an example, Figure 3 presents the axial LF strain, the variation in the elastic modulus M and the variation in the US attenuation α as functions of time, obtained in Berea sandstone. Note that the variations in M and α consist of an offset and a fast modulation at the frequency of the LF resonance. The offset is due to elastic nonlinear conditioning [*Ten Cate and Shankland*, 1996; *Ten Cate et al.*, 2000; *Ten Cate*, 2011; *Renaud et al.*, 2011, also

Table 1. Measured Sample Characteristics

Sample Name	Rock Type	Length (m)	Density (g.cm^{-3})	LF Resonance Frequency (kHz)	LF Damping Ratio (10^{-3})	US P-wave Velocity (km/s)
Grunnes Nidaros soapstone (Norway)	talc schist	0.17	2.9	5.7	4.2	5
Berea sandstone (USA)	fine-grained argillaceous micaceous sandstone	0.15	2.2	4.5	4.5	2.4
Fontainebleau sandstone (France)	pure quartz sandstone	0.19	2.1	1.9	11	1.4
Meule sandstone (red) (France)	fine-grained argillaceous micaceous sandstone	0.12	2.2	5.1	7.6	3
Meule sandstone (gray) (France)	fine-grained argillaceous micaceous sandstone	0.4	2.1	1.6	8.6	3
Sander sandstone (Germany)	sub-arkose sandstone	0.17	2.2	4	8.7	2.9
Pietra Serena sandstone (Italy)	graywacke sandstone	0.17	2.6	4.8	8.1	3.6
Berkeley blue granite (USA)	medium grained anorthosite (crystalline rock)	0.16	2.7	4	7.1	2.9
Lavoux limestone (France)	pelletoidal limestone	0.3	2	2.8	1.1	2.9
Pietra di Vicenza limestone (Italy)	bioclastic limestone	0.18	2	4.5	1.9	3.7
Portland limestone (USA)	oolitic limestone	0.16	2	4.9	1.4	3.4
aluminium		0.19	2.7	6.6	0.8	6

Reversible modification of nonlinear elastodynamics induced by acoustical self-conditioning in limestone, submitted to *Journal of the Acoustical Society of America*, 2011], and will be addressed later.

[7] The synchronization of the LF and US signals allows one to create figures relating $\Delta M(\epsilon_{LF})/M_0$ and $\alpha(\epsilon_{LF}) - \alpha_0$ as a function of ϵ_{LF}, two signatures of elastic nonlinearity. The behavior of the elastic nonlinearity measured in rocks is complex as we shall see. Thus we use an approach that allows us to simplify analysis but nonetheless interpret the nonlinear elastic response. In particular, note that this approach does not provide a quantification of hysteresis. We fit nonlinear elasticity and nonlinear dissipation as functions of the LF strain by applying a second-order polynomial fit:

$$\frac{\Delta M(\epsilon_{LF})}{M_0} \approx C_E + \beta_E\,\epsilon_{LF} + \delta_E\,\epsilon_{LF}^2, \tag{6}$$

$$\alpha(\epsilon_{LF}) - \alpha_0 \approx C_D + \beta_D\,\epsilon_{LF} + \delta_D\,\epsilon_{LF}^2, \tag{7}$$

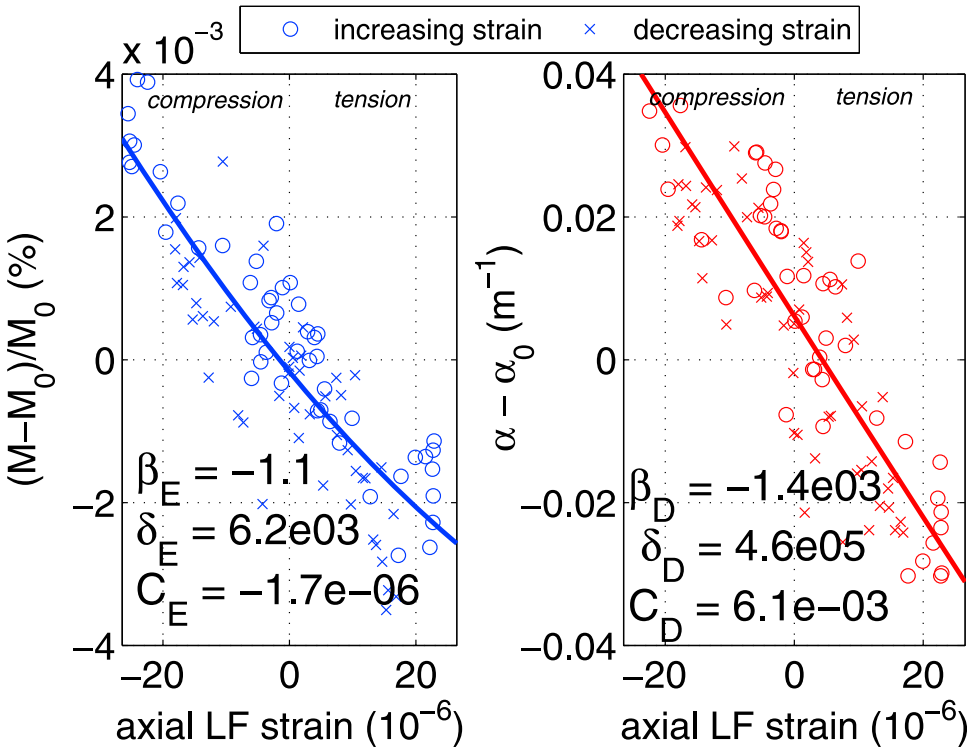

Figure 4. Variation in the elastic modulus and variation in the US attenuation as functions of the LF strain in aluminium at 2.5 × 10^{-5} LF stain amplitude. Circles: increasing strain. Crosses: decreasing strain. Aluminium is used as a standard to compare elasticity with rock samples.

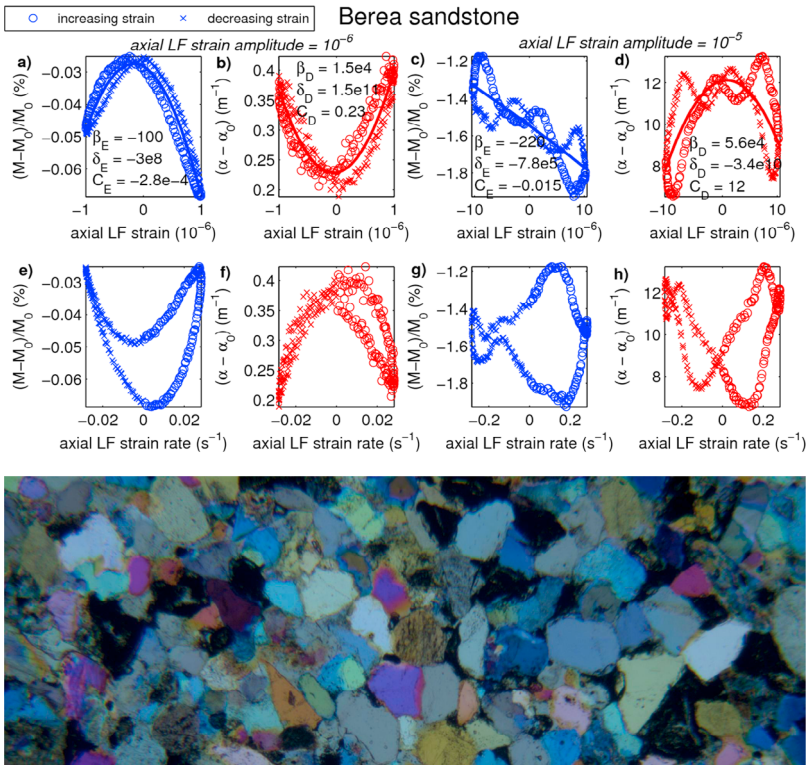

Figure 5. Berea sandstone. (a–d) Variation in the elastic modulus M and variation in the US attenuation α as functions of the axial LF strain for 1×10^{-6} and 1×10^{-5} axial LF strain amplitudes. Solid lines represent quadratic fits and associated nonlinear parameters are displayed. (e–h) Variation in the elastic modulus M and variation in the US attenuation α as functions of the axial LF strain rate for 1×10^{-6} and 1×10^{-5} axial LF strain amplitudes. A photomicrograph of the rock under plane polarized light is shown at the bottom (width of the photo is 2.35 mm). A positive axial LF strain corresponds to axial tension while a negative axial LF strain represents an axial compression.

where C_E quantifies the offset of the modulation in the elastic modulus due to nonlinear material conditioning and where β_E and δ_E are the classical nonlinear elastic parameters for quadratic and cubic elastic nonlinearities, respectively [*Johnson et al.*, 1996]. These parameters are defined for materials exhibiting classical nonlinear behavior due to atomic anharmonicity [*Landau and Lifshitz*, 1986; *Zarembo and Krasil'nikov*, 1971]. As noted, the elastic nonlinearity in rock is dominated by material damage in the form of cracks and other features, but it provides insight to apply the classical formulation for comparison between samples as a first step toward a full nonlinear characterization. For an isotropic solid, β_E is related to the two second-order elastic constants λ and μ, and the three third-order elastic constants l, m and n [*Hamilton and Blackstock*, 1998; *Hughes and Kelly*, 1953]:

$$\beta_E = -\frac{\frac{2}{\lambda+\mu}[l\mu - \lambda(m+\lambda+2\mu)]}{\lambda+2\mu}. \quad (8)$$

Nonlinear dissipation is similarly characterized by the three parameters C_D, β_D and δ_D. Applying the US pulses propagating across the sample, the elastic modulus we probe is the compressional modulus $M = \lambda + 2\mu$, where λ and μ are the second-order elastic constants of Lamé, related to the velocity of compressional waves for an unbounded propagation in an isotropic solid. A positive axial LF strain corresponds to a tensile axial strain while a negative axial LF strain represents a compressive axial strain.

3. Nonlinear Elasticity of 11 Rock Samples

3.1. Sample Descriptions

[8] Table 1 summarizes the characteristics of the room-dry rock samples. All the samples are cylindrical and have a diameter of 25 mm. An aluminium sample with similar dimensions is used as an elastically linear standard material to calibrate the experimental setup. The US attenuation for frequencies between 1 MHz and 2 MHz is dominated by scattering in dry rocks; it ranges from 20 to 1000 m^{-1} [*D'Angelo et al.*, 2008] which corresponds to a quality factor varying from 1 to 100.

3.2. Aluminium as Elastically Linear Standard

[9] Due to the Poisson effect, the dynamic axial LF strain produces a radial dynamic displacement. This induces modulations in the TOF and the amplitude of the US pulses that are unwanted artifacts (since there are not created by the elastic nonlinearity of the material). In addition, the dynamic variation in the density of the material also induces a modulation in the speed of sound [*Renaud et al.*, 2011]. In order to quantify these effects, we use as a standard an aluminium

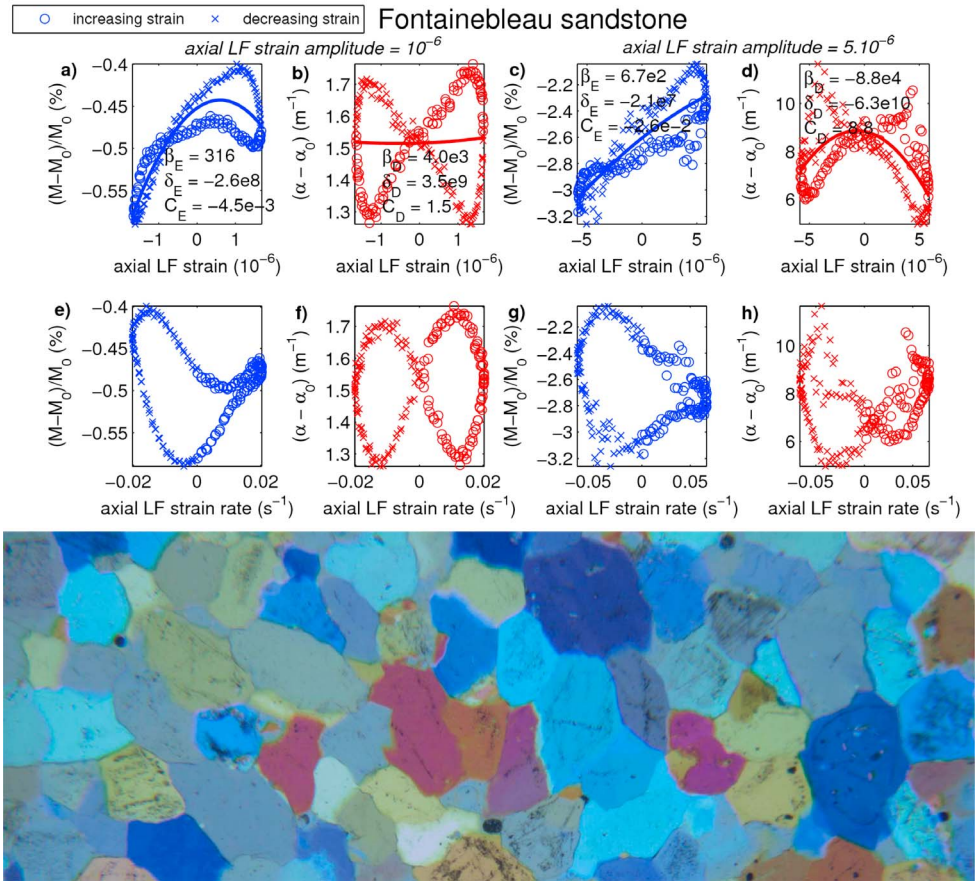

Figure 6. Fontainebleau sandstone. Same conventions as in Figure 5. The width of the photomicrograph is 2.35 mm.

sample which exhibits a very weak classical quadratic elastic nonlinearity and no significant amplitude-dependent dissipation. Figure 4 shows the variations in the elastic modulus and in the US attenuation as functions of the LF strain for a LF strain amplitude of 2.5×10^{-5} measured in aluminium. These variations are partly artifactual. We observe no offset (no variation at zero LF strain meaning $C_E = 0$) and a linear relationship (tension-compression symmetry) in aluminium. We measure $\beta_E = -1.1$. This is of the same order of magnitude as values reported in literature measured by quasi-static acousto-elastic testing [*Smith et al.*, 1966; *Sarma and Reddy*, 1972] that can be positive or negative and are lower than 5 in absolute value, depending on the aluminium alloy. The value of β_E must however be corrected for the Poisson and density effects to isolate the acoustoelastic effect [*Renaud et al.*, 2011]. Indeed, we showed in a previous study [*Renaud et al.*, 2011] that roughly one third of the TOFM is actually due to the acoustoelastic effect when the US pulses propagate along the surface of the aluminium sample, in the same direction as the LF loading. In the present experimental configuration, the acoustoelastic effect is weaker because the US pulses propagate in a direction perpendicular to that of the LF stress [*Hughes and Kelly*, 1953], therefore the contribution of the acoustoelastic effect to the total measured TOFM is even smaller. In short, we take a practical approach. We use the values of the nonlinear parameters obtained in aluminium (see Figure 4) as baselines indicating the level of these artifacts. The nonlinear parameters measured in rocks (section 3.3) are at least ten times larger than the values of the nonlinear parameters measured in aluminium, and therefore we deem the artifactual sources negligible when analyzing the results in the rock samples.

3.3. Results in 11 Rock Samples

[10] Figures 5–15 present the results obtained in 11 different rock samples at moderate and high strain amplitudes of 1×10^{-6} and 1×10^{-5} (note that due to high dissipation in some rocks, we were only able to generate a LF strain amplitude of 5×10^{-6} rather than 1×10^{-5}). Figure 16 summarizes the values of the nonlinear parameters measured for the 11 rock samples and for the two investigated LF strain amplitudes.

[11] We find that, Grunnes soapstone and all poly mineralogic sandstones depict similar elastic nonlinear behaviors. They exhibit responses showing varying degrees of hysteresis and large cubic nonlinearity ($\delta_E \gg \beta_E^2$ and $\delta_D \gg \beta_D^2$). The material softens under both axial compression and axial tension but hardens near zero pressure at 1×10^{-6} LF strain amplitude. At 1×10^{-5} LF strain amplitude, more elaborate hysteretic signatures are measured. In contrast, pure quartz

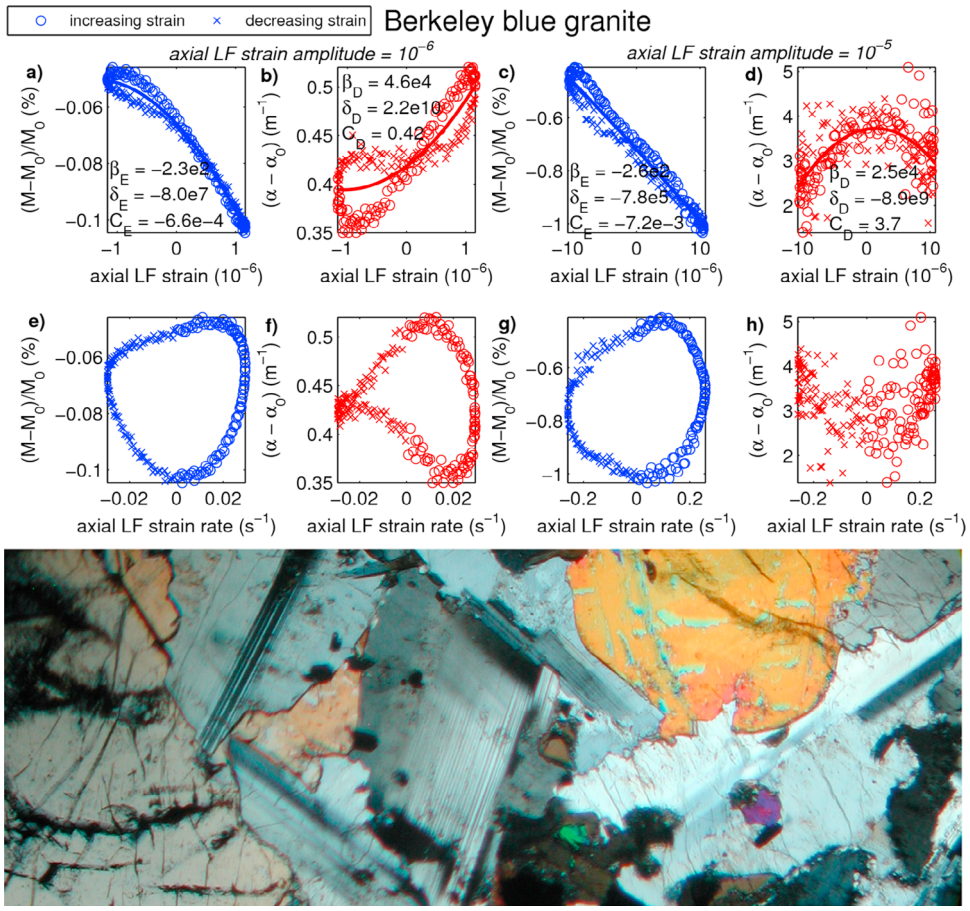

Figure 7. Berkeley blue granite. Same conventions as in Figure 5. The width of the photomicrograph is 3.85 mm.

Fontainebleau sandstone manifests anomalous nonlinear elasticity, indeed β_E has a tremendously high value ($\beta_E = 670$ at 5×10^{-6} LF strain amplitude) and is positive, meaning that the speed of sound decreases during axial compressive strain and increases under axial tensile strain (Figure 6). The opposite behavior is observed in a large majority of Earth solids. Why this is the case in light of the behaviors in the other rock samples is currently not understood although Fontainebleau has historically shown exotic elastic behaviors [e.g., *Zinszner et al.*, 1997; *Pasqualini et al.*, 2007]. In the sample of Berkeley blue granite, the material hardens progressively as the axial compression increases and softens progressively under dilation. We measure a strong quadratic elastic nonlinearity and hysteresis as well (Figure 7). As for limestone samples, Lavoux limestone exhibits weak nonlinear responses whereas Portland limestone (Figure 12) and Pietra di Vicenza limestone (Figure 13) show significant nonlinear behaviors with hystereses that are markedly different than those measured in sandstones. Hystereses in limestones are open loops with a 'banana-like' shape.

[12] The observed curvature of the normed elastic modulus as a function of the strain amplitude in many of the sandstones points to a particular behavior. This indicates that the features responsible for the elastic nonlinearity 'lock' near zero pressure (when viscous forces due to grain-cement interaction or thin films adsorbed on grain surfaces are maximum since the strain rate is maximum) but activate as amplitude increases in both senses to reach a maximum variation at the maximum strain, when the viscous forces are reduced since the strain rate is null. Shear along an ensemble of cracks could behave in this manner and we speculate that this may be the case. In the limestones and granite, the modulus-strain shows softening only in tension. Such behavior may come from activating opening and closing of cracks that dominate the behavior as opposed to shearing. This type of behavior is known as 'clapping' [e.g., *Solodov*, 1998]. One can also imagine a shearing mechanism that is symmetric in contrast to shearing in the sandstones where both compression and tension soften the material.

[13] Recently, there have been observations of Earth processes that appear to be associated with strain rate rather than strain. For instance, observations of tidal forcing of tremor in Cascadia by *Hawthorne and Rubin* [2010] as well as deformation in the Guerrero gap in Mexico associated with slow slip [*Rivet et al.*, 2011] show that strain rate seems to be the controlling parameter. Historically, acoustic and elastic nonlinearity have been shown to depend on the strain based on observation and physics-based theories [e.g., *Hamilton and Blackstock*, 1998; *Zarembo and Krasil'nikov*, 1971;

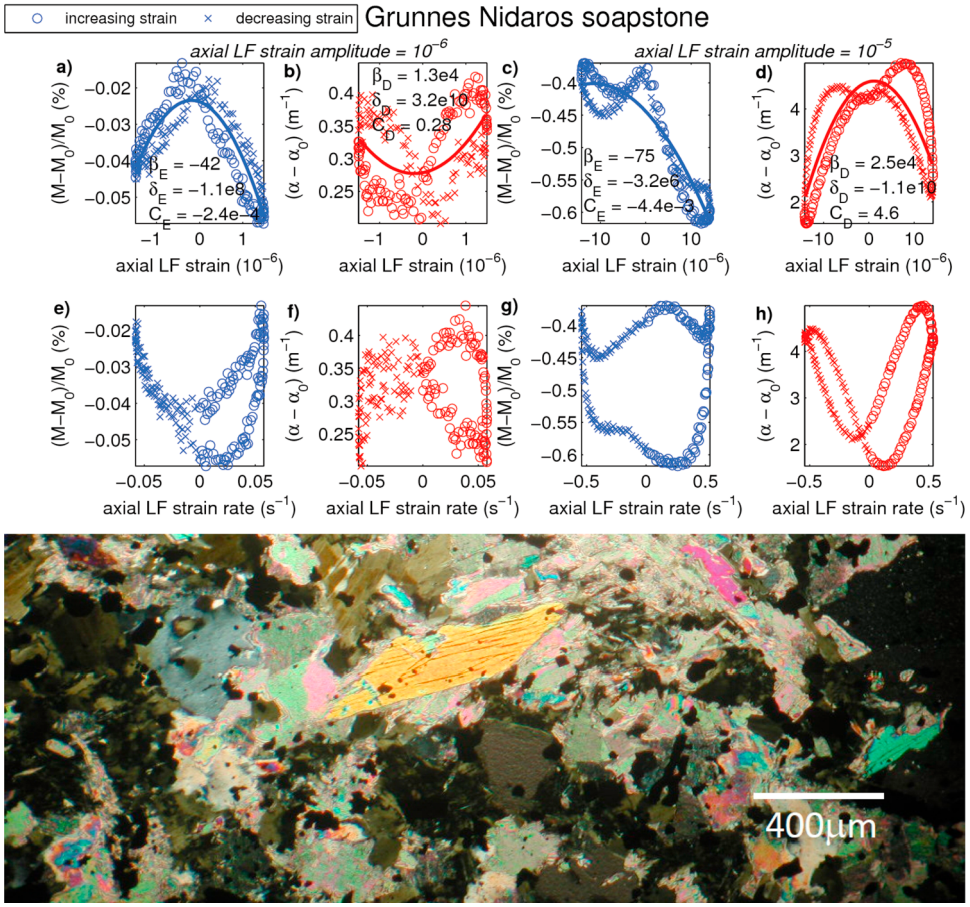

Figure 8. Grunnes Nidaros soapstone. Same conventions as in Figure 5.

Guyer and Johnson, 2009]. However, strain rate is extremely important in regards to the magnitude of the hysteresis. In general, it has been shown that as strain rate goes to zero, the hysteresis goes to zero [*Claytor et al.*, 2009]. We present both strain and strain rate dependencies here in order to compare and contrast the two. Plotting data as function of strain rate also helps isolate viscous effects.

[14] As reported in *Ten Cate and Shankland* [1996], *Ten Cate et al.* [2000], *Pasqualini et al.* [2007], and Renaud et al. (submitted manuscript, 2011), dynamically induced conditioning is usually significant for strain amplitudes above approximately 10^{-6} in rocks (it is a material dependent effect). It brings the material to a non-equilibrium, metastable state and modifies its nonlinear elasticity. The variations in M and α measured with DAET consist of an offset (C_E and C_D) and a fast modulation at the frequency of the LF resonance (characterized by β_E, β_D, δ_E and δ_D). The offsets C_E and C_D provide a measure of the magnitude of the conditioning. In short, when the sample is still in the elastic nonlinear regime, but below the non-equilibrium regime (first and second regimes respectively of *Pasqualini et al.* [2007]), $C_E = 0$ and $C_D = 0$. A soon as the sample enters the second regime, $C_E < 0$ and $C_D > 0$. For all of the 11 investigated rocks, when increasing the LF strain amplitude from 10^{-6} to 10^{-5}, the absolute values of β_E, β_D, C_E and C_D increase whereas the absolute values of δ_E and δ_D decrease (Figure 16). The effects of conditioning have been carefully explored in *Pasqualini et al.* [2007] and *Ten Cate* [2011] applying Nonlinear Resonant Ultrasound Spectroscopy which averages the nonlinear behavior over many wave cycles. These studies showed that conditioning is important at strains that depend on the material, it becomes significant for strain amplitudes above 5×10^{-7} in sandstones under fixed temperature and pressure (this is equivalent to saying the material traverses the boundary between first and second regimes into metastability). Our work is in agreement with these observations. However, what is masked in the *Pasqualini et al.* [2007] study and others that employ NRUS are the exotic behaviors in modulus-strain over a single pressure cycle as shown in Figures 5–15.

3.4. Reproducibility of Dynamic Acoustoelastic Testing in *5* Rocks

[15] In order to test the reproducibility of DAET, we repeated the identical protocol over a three day period. This protocol consisted of performing DAET such that the US wave probes a sample at the same position along its axis but at 3 different angles (0°, 45° and 90°, in the plane perpendicular to the long axis of the sample), for 5 rock samples. The samples were detached from the LF source and repositioned every day. Thus 9 DAET measurements are conducted for each rock sample. Figure 17 shows the average

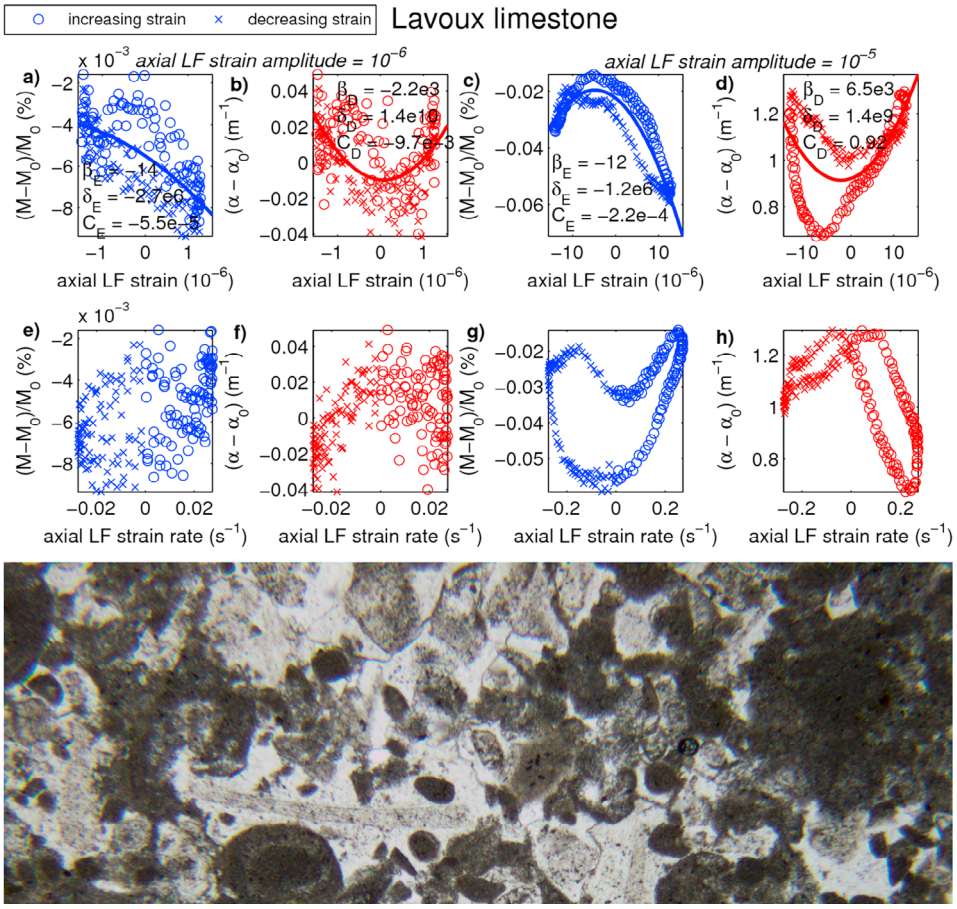

Figure 9. Lavoux limestone. Same conventions as in Figure 5. The width of the photomicrograph is 2.35 mm.

value and the standard deviation obtained for the 6 nonlinear parameters and for each rock sample. The standard deviation ranges from 10% to 60%, except for β_E and β_D in Pietra di Vicenza limestone likely due to heterogeneity of the sample. We note that elastic anisotropy may affect these observations as well. Temperature and humidity were not controlled and the lesson may well be that they must be in order to quantify repeatability.

4. Discussion

[16] One goal was to compare the granite, with known microstructure, to the other samples. The granite hardens through compression and softens under tension. The limestones reflect this behavior as well. This behavior is related to the crack response, slip that is highly reversible is our current hypothesis. In contrast, many of the sandstones show softening in compression and tension, with a minimum effect at zero strain. These materials may have sliding that is arrested at zero strain in a manner to be determined. The interpretations may be made independent of the vastly different mineralogy and internal geometry of the samples. This is highly satisfying. We will also continue studying other rock types to build our catalog of elastic behaviors in Earth materials. Further, we are in the process of developing a physics-based description of the behaviors we observe. Applying this model we hope to develop a quantitative link between the elaborate elastic nonlinearity and the defect geometry and concentration. Beyond this, the idea will be to include the effects of moisture, pressure and temperature in such a model.

5. Conclusions

[17] We described observations applying a new probe termed dynamic acoustoelastic testing, to characterize the complex dynamic elastic behavior of, in this case, room-dry rock samples. The method provides the means to dynamically study the velocity-strain and attenuation-strain behaviors through the full wave cycle in contrast to most methods that measure average response. The method relies on exciting a sample with a low frequency vibration in order to cycle it through stress-strain multiple times. Simultaneously, a high frequency ultrasonic source applies pulses and the change in wave speed as a function of the low frequency strain is measured. Nine sedimentary, one crystalline and one metamorphic rock samples with different mineral constituents and microstructures were investigated. In the crystalline rock, we observed a high quadratic elastic nonlinearity which may arise from the microcracks and

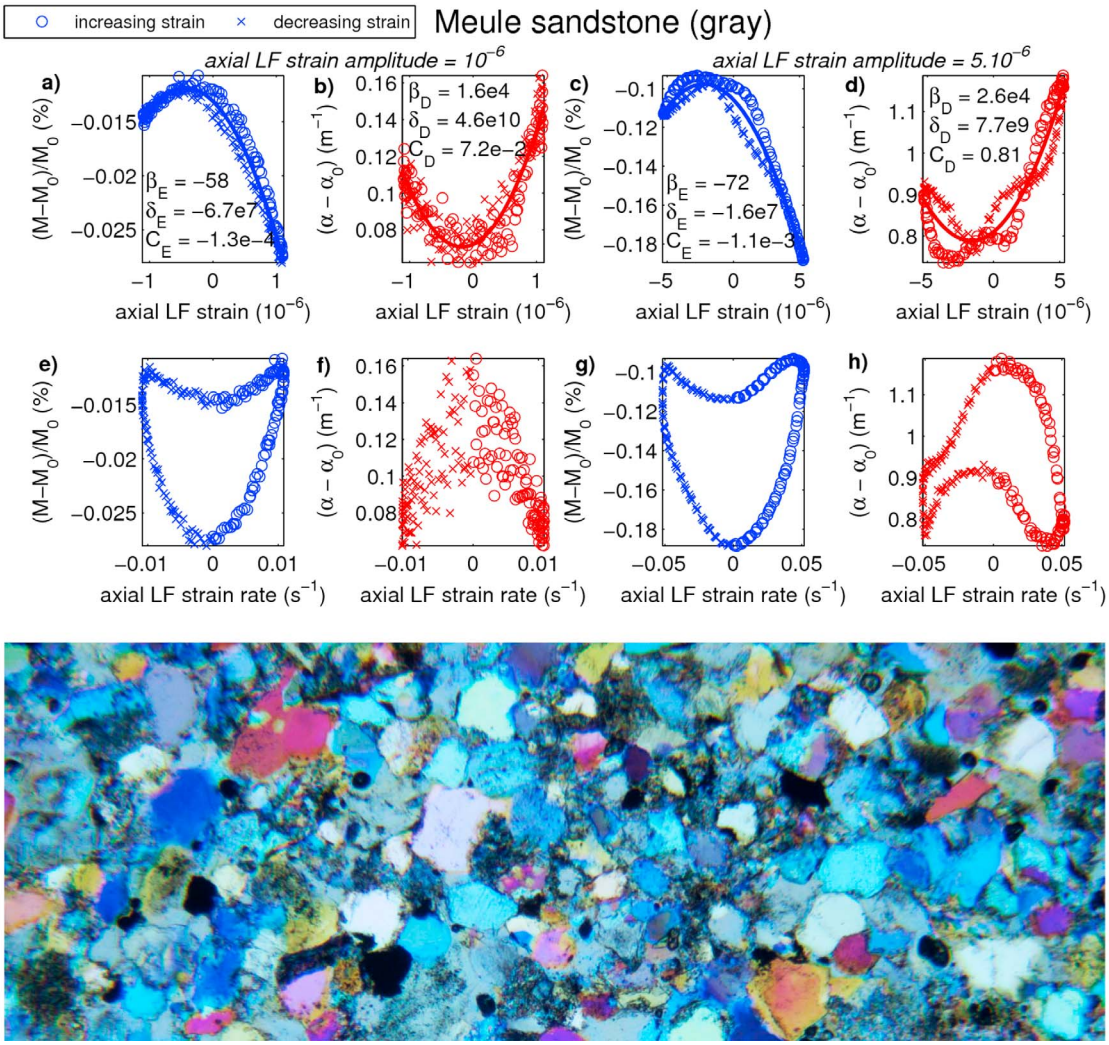

Figure 10. Meule sandstone (gray). Same conventions as in Figure 5. The width of the photomicrograph is 2.35 mm.

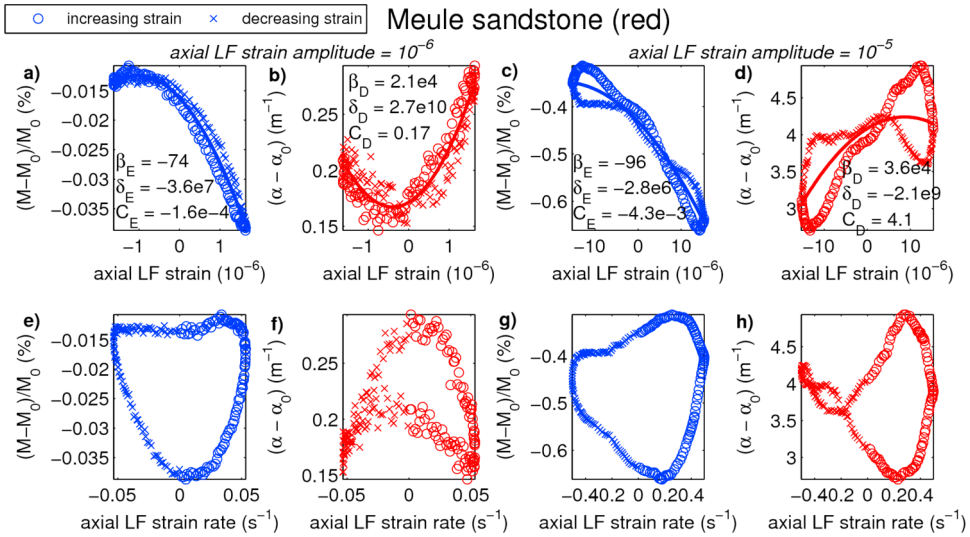

Figure 11. Meule sandstone (red). Same conventions as in Figure 5.

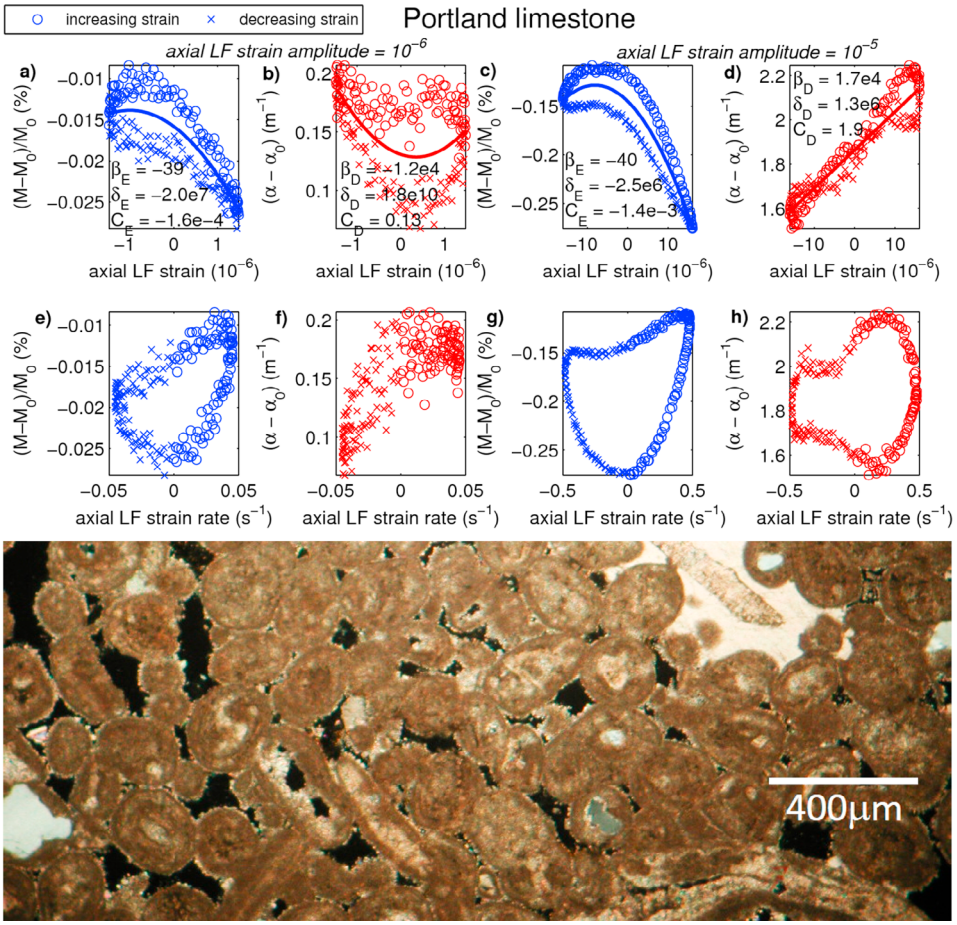

Figure 12. Portland limestone. Same conventions as in Figure 5.

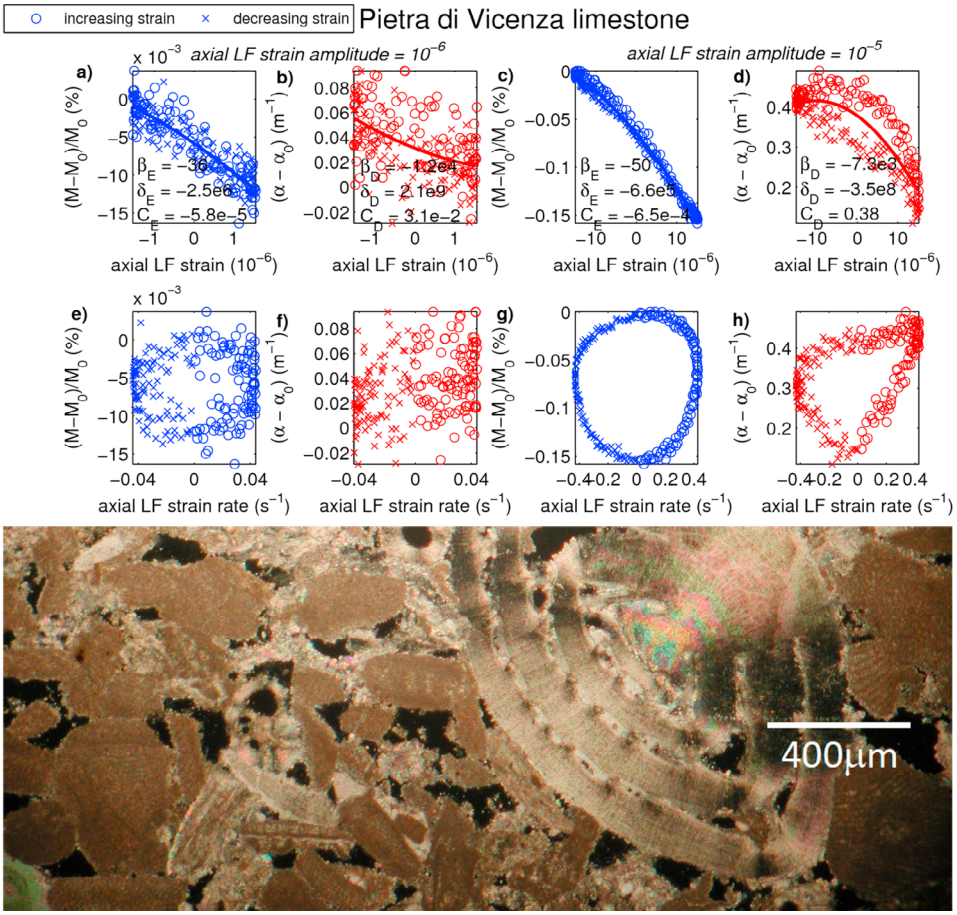

Figure 13. Pietra di Vicenza limestone. Same conventions as in Figure 5.

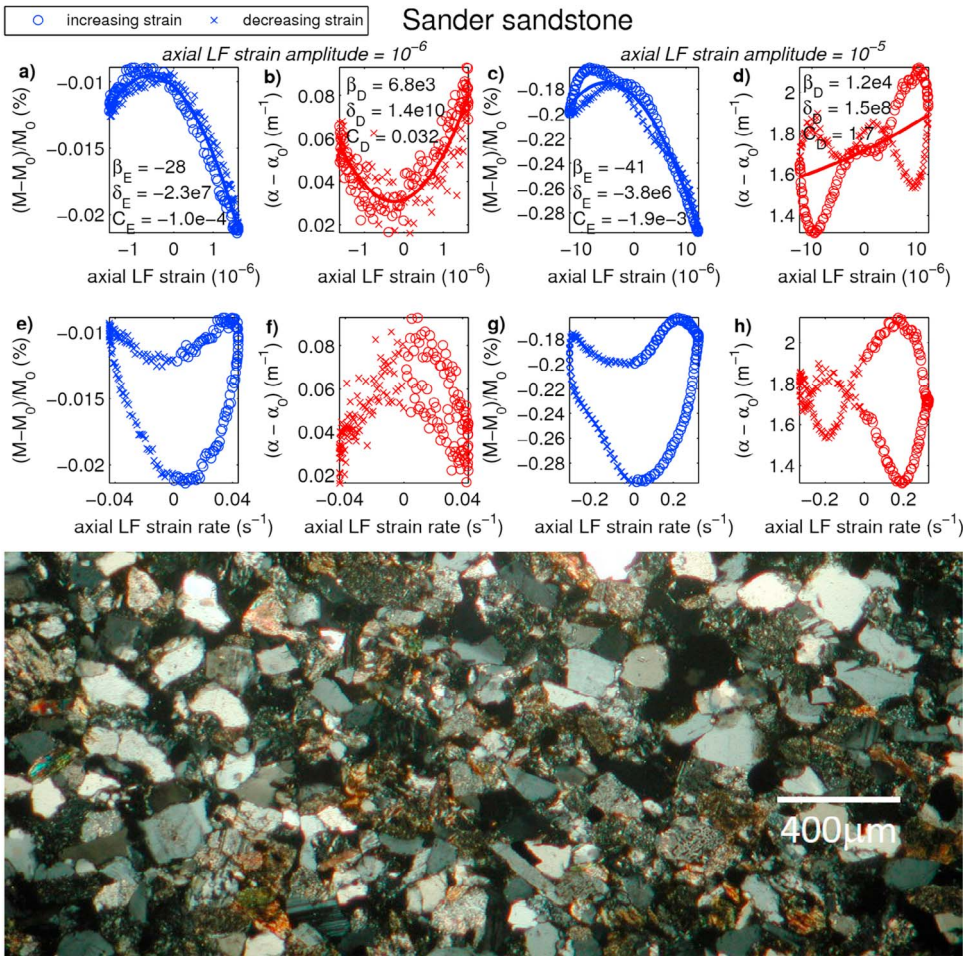

Figure 14. Sander sandstone. Same conventions as in Figure 5.

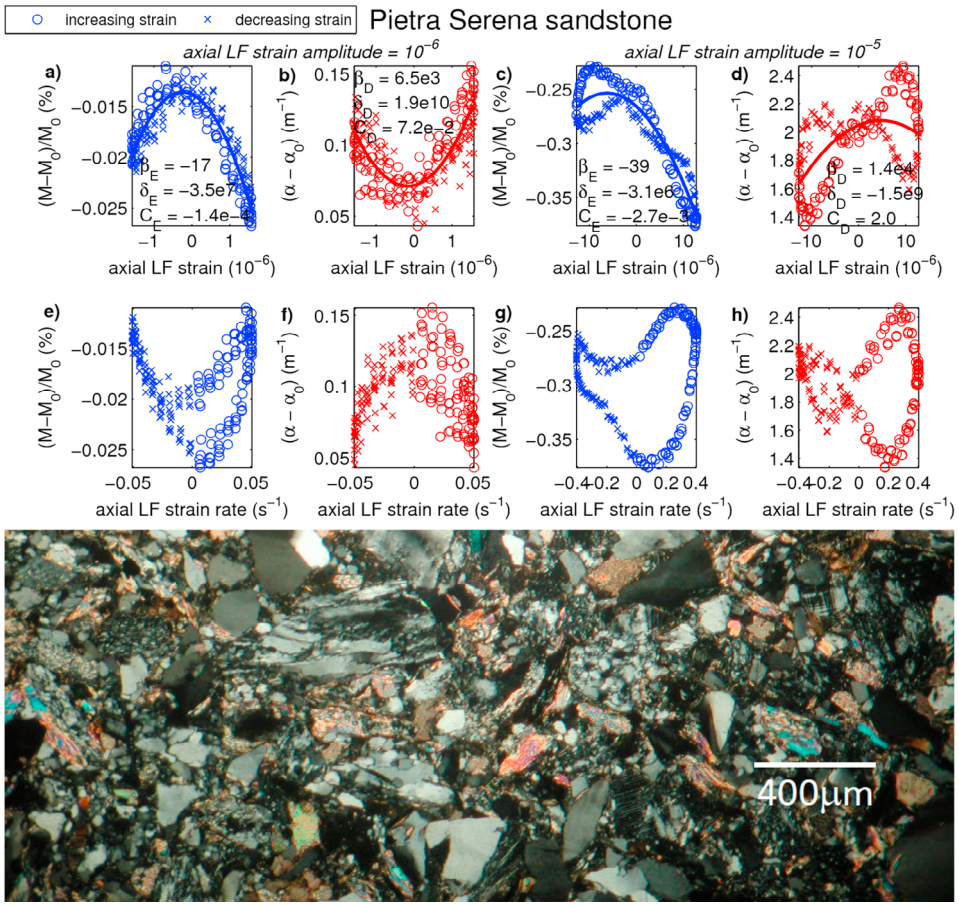

Figure 15. Pietra Serena sandstone. Same conventions as in Figure 5.

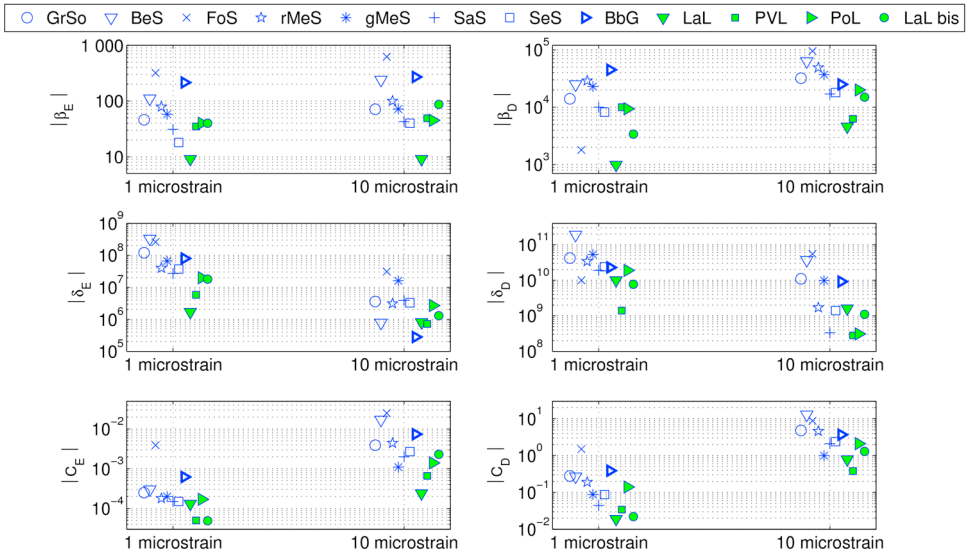

Figure 16. Summary of the nonlinear parameters (in absolute value) measured in the 11 rock samples at 1×10^{-6} and 1×10^{-5} LF stain amplitudes for the (left) elastic modulus parameters and (right) attenuation parameters. The results of a previous study in a different sample of Lavoux limestone [*Renaud et al.*, 2011] is also reported. GrSo: Grunnes soapstone, BeS: Berea sandstone, FoS: Fontainebleau sandstone, rMeS: red Meule sandstone, gMeS: gray Meule sandstone, SaS: Sander sandstone, SeS: Serena sandstone, BbG: Berkeley blue granite, LaL: Lavoux limestone, PVL: Pietra di Vicenza limestone, PoL: Portland limestone, LaL bis: Lavoux limestone (data from *Renaud et al.* [2011, also submitted manuscript, 2011]).

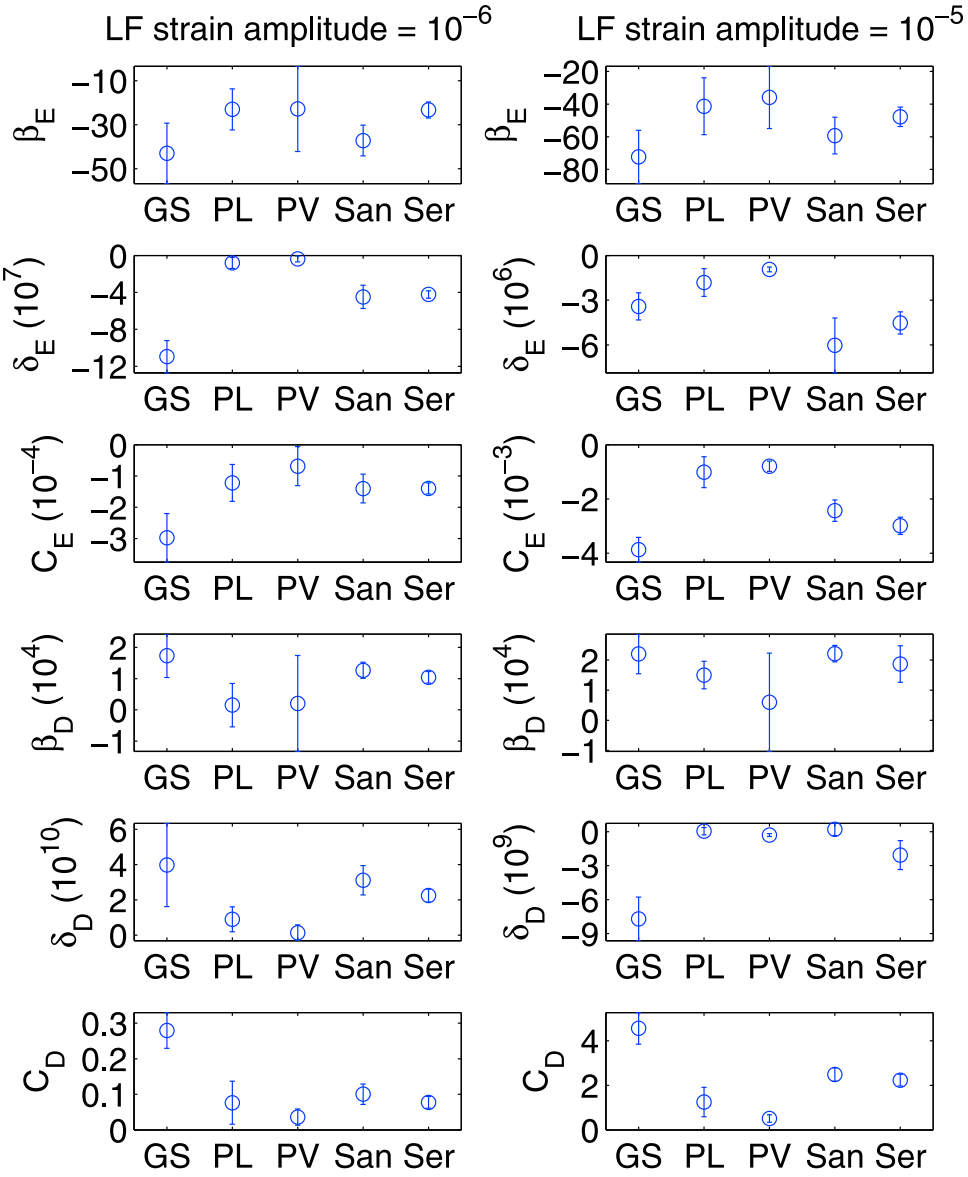

Figure 17. Average value and standard deviation of nonlinear parameters measured in 5 rock samples when DAET is repeated 9 times. GS: Grunnes soapstone, PL: Portland sandstone, PV: Pietra di Vicenza limestone, San: Sander sandstone, Ser: Serena sandstone.

dislocations contained within individual crystals. In contrast, at low strain amplitude (10^{-6}), sandstones and the metamorphic rock showed similar behaviors; both axial compression and axial tension produced a softening of the material and enhanced the ultrasound attenuation. We also observed that, for all rock samples, acoustically induced conditioning induced a reversible change in the nonlinear elastic behavior. Our short and long term goal is to characterize the physical mechanisms responsible for the observed elastic nonlinear behaviors. We will do this applying numerical modeling and frictional models. The information provided by this technique has significant implication for the development of a physics-based theory, and thus ultimately to our ability to directly relate nonlinear elastic behavior to damage and microstructure features in Earth materials.

[18] **Acknowledgments.** We gratefully acknowledge the support of the U.S. Department of Energy, Office of Basic Energy Research. The authors thank Koen van den Abeele and Bart van Damme (K.U. Leuven Campus Kortrijk, Belgium) and Ton van der Steen (Erasmus Medical Center, Rotterdam, Netherlands). We acknowledge the European project Integrated tool for in situ characterization of effectiveness and durability of conservation techniques in historical structures (DIAS) (DIAS-EVK4-CT-2002-00080). We also thank T.J. Ulrich and J.A. TenCate for discussions and experimental assistance.

References

Céspedes, I., Y. Huang, J. Ophir, and S. Spratt (1995), Methods for estimation of subsample time delays of digitized echo signals, *Ultrason. Imaging*, *17*, 142–171.

Claytor, K. E., J. R. Koby, and J. A. TenCate (2009), Limitations of preisach theory: Elastic aftereffect, congruence, and end point memory, *Geophys. Res. Lett.*, *36*, L06304, doi:10.1029/2008GL036978.

D'Angelo, R., K. Winkler, and D. Johnson (2008), Three wave mixing test of hyperelasticity in highly nonlinear solids: Sedimentary rocks, *J. Acoust. Soc. Am.*, *123*(2), 622–639.

Gremaud, G., M. Bujard, and W. Benoit (1987), The coupling technique: A two-wave acoustic method for the study of dislocation dynamics, *J. Appl. Phys.*, *61*(5), 1795–1805.

Guyer, R., and P. Johnson (2009), *Nonlinear Mesoscopic Elasticity*, 396 pp., John Wiley, Weinheim, Germany.

Hamilton, M., and D. Blackstock (1998), *Nonlinear Acoustics, Theory and Applications*, 455 pp., Academic Press, New York.

Hawthorne, J., and A. Rubin (2010), Tidal modulation of slow slip in cascadia, *J. Geophys. Res.*, *115*, B09406, doi:10.1029/2010JB007502.

Hughes, D., and J. Kelly (1953), Second-order elastic deformation of solids, *Phys. Rev.*, *92*(5), 1145–1149.

Johnson, P., B. Zinszner, and P. Rasolofosaon (1996), Resonance and elastic nonlinear phenomena in rock, *J. Geophys. Res.*, *101*(B5), 11,553–11,564.

Landau, L., and E. Lifshitz (1986), *Theory of Elasticity*, 3rd ed., 195 pp., Butterworth-Heinemann, Oxford, U. K.

Moreschi, H., S. Callé, S. Guerard, D. Mitton, G. Renaud, and M. Defontaine (2010), Monitoring trabecular bone microdamage using a dynamic acousto-elastic testing method, in *Proceedings of the Institution of Mechanical Engineers, Part H: Journal of Engineering in Medicine*, pp. 1–14, Inst. Mech. Eng., London.

Nagy, P. (1998), Fatigue damage assessment by nonlinear ultrasonic materials characterization, *Ultrasonics*, *36*(1–5), 375–381.

Pasqualini, D., K. Heitmann, J. TenCate, S. Habib, D. Higdon, and P. Johnson (2007), Nonequilibrium and nonlinear dynamics in berea and fontainebleau sandstones: Low-strain regime, *J. Geophys. Res.*, *112*, B01204, doi:10.1029/2006JB004264.

Renaud, G., S. Callé, J.-P. Remenieras, and M. Defontaine (2008), Exploration of trabecular bone nonlinear elasticity using time-of-flight modulation, *IEEE Trans. Ultrason. Ferroelectr. Freq. Control*, *55*(7), 1497–1507.

Renaud, G., S. Callé, and M. Defontaine (2009), Remote dynamic acoustoelastic testing: Elastic and dissipative acoustic nonlinearities measured under hydrostatic tension and compression, *Appl. Phys. Lett.*, *94*, 011905, http://dx.doi.org/10.1063/1.3064137.

Renaud, G., M. Talmant, S. Callé, M. Defontaine, and P. Laugier (2011), Nonlinear elastodynamics in micro-inhomogeneous solids observed by head-wave based dynamic acoustoelastic testing, *J. Acoust. Soc. Am.*, *130*(6), 3583–3589.

Rivet, D., M. Campillo, N. Shapiro, V. Cruz-Atienza, M. Radiguet, N. Cotte, and V. Kostoglodov (2011), Seismic evidence of nonlinear crustal deformation during a large slow slip event in mexico, *Geophys. Res. Lett.*, *38*, L08308, doi:10.1029/2011GL047151.

Sarma, V., and P. Reddy (1972), Third-order elastic constants of aluminium, *Phys. Status Solidi A*, *10*(2), 563–567.

Smith, R. T., R. Stern, and R. Stephens (1966), Third-order elastic moduli of polycrystalline metals from ultrasonic velocity measurements, *J. Acoust. Soc. Am.*, *40*(5), 1002–1008.

Solodov, I. (1998), Ultrasonics of non-linear contacts: Propagation, reflection and nde-applications, *Ultrasonics*, *36*(1–5), 383–390.

Ten Cate, J. (2011), Slow dynamics of earth materials: An experimental overview, *Pure Appl. Geophys.*, *168*, 2211–2219.

Ten Cate, J., and T. Shankland (1996), Slow dynamics in the nonlinear elastic response of berea sandstone, *Geophys. Res. Lett.*, *23*, 3019–3022.

Ten Cate, J., E. Smith, and R. Guyer (2000), Universal slow dynamics in granular solids, *Phys. Rev. Lett.*, *85*(5), 1020–1023.

Winkler, K., and L. McGowan (2004), Nonlinear acoustoelastic constants of dry and saturated rocks, *J. Geophys. Res.*, *109*, B10204, doi:10.1029/2004JB003262.

Zarembo, L., and V. Krasil'nikov (1971), Nonlinear phenomena in the propagation of elastic waves in solids, *Sov. Phys. Usp., Engl. Transl.*, *13*(6), 778–797.

Zinszner, B., P. Johnson, and P. Rasolofosaon (1997), Influence of change in physical state on the elastic nonlinear response in rock: Significance of effective pressure and water saturation, *J. Geophys. Res.*, *102*(B4), 8105–8120.